A. Tempelhahn, H. Budzier, V. Krause, G. Gerlach

# Improving the shutter-less compensation method for TEC-less microbolometer-based infrared cameras

**Erstveröffentlichung in / First published in:**

*SPIE Defense + Security*. Baltimore, 2015. Bellingham: SPIE, Vol. 9451 *[Zugriff am: 02.05.2019].*

DOI: https://doi.org/10.1117/12.2177003

PROCEEDINGS OF SPIE

SPIEDigitalLibrary.org/conference-proceedings-of-spie

# Improving the shutter-less compensation method for TEC-less microbolometer-based infrared cameras

A. Tempelhahn, H. Budzier, V. Krause, G. Gerlach

A. Tempelhahn, H. Budzier, V. Krause, G. Gerlach, "Improving the shutter-less compensation method for TEC-less microbolometer-based infrared cameras," Proc. SPIE 9451, Infrared Technology and Applications XLI, 94511F (8 June 2015); doi: 10.1117/12.2177003

SPIE.

Event: SPIE Defense + Security, 2015, Baltimore, Maryland, United States

# Improving the shutter-less compensation method for TEC-less microbolometer-based infrared cameras

A. Tempelhahn*, H. Budzier, V. Krause, G. Gerlach,
Solid-State Electronics Laboratory, Technische Universität Dresden, 01062 Dresden, Germany

## ABSTRACT

Shutter-less infrared cameras based on microbolometer focal plane arrays (FPAs) are the most widely used cameras in thermography, in particular in the fields of handheld devices and small distributed sensors. For acceptable measurement uncertainty values the disturbing influences of changing thermal ambient conditions have to be treated corresponding to temperature measurements of the thermal conditions inside the camera. We propose a compensation approach based on calibration measurements where changing external conditions are simulated and all correction parameters are determined. This allows to process the raw infrared data and to consider all disturbing influences. The effects on the pixel responsivity and offset voltage are considered separately. The responsivity correction requires two different, alternating radiation sources. This paper presents the details of the compensation procedure and discusses relevant aspects to gain low temperature measurement uncertainty.

**Keywords:** microbolometer, FPA, thermal drift compensation, shutter-less, TEC-less

## 1. INTRODUCTION

Microbolometer-based infrared cameras are used in many fields of application, e.g. in quality control during production processes, fire protection, and surveillance. Their benefits are low power consumption due to uncooled thermal infrared sensors, compact size and low costs compared to infrared cameras based on cooled photon detectors. The latest improvements in the microfabrication process of microbolometer focal plane arrays (FPAs) in terms of pixel pitch lead to increased spatial resolution but reduced sensor size. The decreasing sensor cost is another reason why infrared thermography enters new fields of application, e.g. in smart phone devices or as sensors for smart building control systems.

Changing thermal conditions inside the camera are the main cause of measurement uncertainty. These changes are due to the changing ambient temperature and the resulting heat transfer processes. Two different aspects have to be considered in order to achieve low measurement uncertainty: (i) changing disturbing radiation derived from the camera interior and (ii) changing sensor parameters (responsivity and offset voltage). The common approach used in former state-of-the-art infrared cameras is based on an optical shutter and temperature-stabilized senor array [1, 2]. The shutter is used for runtime recalibration purposes in order to overcome changes of the disturbing radiation, whereas a thermoelectric cooler (TEC) keeps the detector on a certain temperature. The disadvantages of the shutter are an interrupted measurement due to the recalibration procedure and the size limitation of the camera coming along with the fact that the shutter has to cover the entire aperture. The high power consumption due to the temperature stabilization is another disadvantage of these infrared cameras which lead to new correction methods. In [3, 4] an approach is presented to overcome the thermal drift influences on the sensor parameters of infrared cameras without TEC. The presented correction method is based on the established shutter correction. With the use of a heating chamber the ambient temperature is controlled and correction parameters based on the sensor temperature are determined. In [5] a shutter-less offset correction for temperature stabilized infrared cameras has been described. The disturbing radiation is estimated using additional temperature probes inside the camera housing. Another shutter-less thermal drift compensation is proposed in [6] for microbolometer-based FPAs without temperature stabilization using only the sensor temperature as correction input. In [7] a complete different approach is presented for TEC-less and shutter-less infrared cameras. An infrared filter covers periodically the camera field of view (FOV) and enables the responsivity correction. The offset voltage correction is based on scene-based correction algorithms. But this approach is based on the external movable filter which compromised the measurement set-up. This paper studies the new approach of capturing the thermal state of the camera during the measurements and using this information to compensate the disturbing influences of a changing ambient temperature. Relevant aspects to gain a low temperature measurement uncertainty are discussed.

*alexander.tempelhahn@tu-dresden.de; phone +49 351 463 34098; fax +49 351 463 32320; tu-dresden.de

Infrared Technology and Applications XLI, edited by Bjørn F. Andresen,
Gabor F. Fulop, Charles M. Hanson, Paul R. Norton, Proc. of SPIE Vol. 9451,
94511F · © 2015 SPIE · CCC code: 0277-786X/15/$18 · doi: 10.1117/12.2177003

## 2. RADIATION MODEL

Infrared cameras detect radiation emitted by any object with a temperature above absolute zero. The Planck's radiation law describes the emitted spectral radiant flux density $M_{\lambda S}$ depending on the absolute object temperature $T$ and the emitted wavelength $\lambda$ with the constants $c_1 = 3.7418 \times 10^{-16}\ \mathrm{Wm^2}$ and $c_2 = 0.0143877\ \mathrm{mK}$ [1]:

$$M_{\lambda S} = \frac{c_1}{\lambda^5} \frac{1}{e^{\frac{c_2}{\lambda T}} - 1}. \tag{1}$$

The integral of $M_{\lambda S}$ over the working spectral band of the used detector yields the maximum possible emitted radiant flux density. Therefore, it is essential to have knowledge about the emissivity $\varepsilon$ of the observed object which is defined by its material and surface properties. Microbolometer-based FPAs use the temperature dependency of the sensor material to convert the exchanged radiant flux $\Phi_{pix,ij}$ of each pixel $(ij)$ into the pixel signal voltage $V_{pix,ij}$. This linear relation comprises the pixel voltage responsivity $R_{V,ij}$ and the offset voltage $V_{0,ij}$:

$$V_{pix,ij} = R_{V,ij}\left(\vartheta_{fpa}\right)\Phi_{pix,ij} + V_{0,ij}\left(\vartheta_{fpa}\right). \tag{2}$$

Both sensor parameter – responsivity and offset voltage – are pixel-dependent. They vary in certain limits over the sensor array due to little variations during the microfabrication process of the FPA. These variations are equalized by applying a non-uniformity correction (NUC). Additionally, the sensor parameter are related to the sensor temperature $\vartheta_{fpa}$. In [8] it has been shown that the projected solid angle of a pixel $\omega_{fov,pix}$ covers nearly the entire half space $\omega_{hs} \approx \pi$. The camera's field of view (FOV) respectively its projected solid angle $\omega_{fov,cam}$ depends on the *f*-number of the used aperture. State-of-the-art infrared cameras use an *f*-number around unity. In that case, $\omega_{fov,cam}$ yields about one fifth of $\omega_{fov,pix}$. That is the reason why each pixel detects radiation derived from the observed scene and radiation derived from the camera interior. The exchanged radiant flux $\Phi_{pix,ij}$ comprises the pixel area $A_{pix}$ and the radiation parts multiplied by their related projected solid angles $\omega_{fov,ij}L_{obj}$from the observed scene, $\omega_{cam,ij}L_{cam}$ from the camera interior, and the pixel radiant exitance $M_{pix}$ emitted into the entire half space:

$$\Phi_{pix,ij} = A_{pix}\left[\omega_{fov,ij}L_{obj}\left(\vartheta_{obj}\right) + \omega_{cam,ij}L_{cam}\left(\vartheta_{cam}\right) - M_{pix}\left(\vartheta_{fpa}\right)\right]. \tag{3}$$

The pixel location and its distance to the optical axis results in pixel-specific projected solid angles $\omega_{fov,ij}$ and $\omega_{cam,ij}$. Three temperatures respectively temperature distributions are involved: (i) the objects surface temperature $\vartheta_{obj}$ which should be determined, (ii) the camera temperature $\vartheta_{cam}$ and (iii) in close relation to that the sensor temperature $\vartheta_{fpa}$.

Changes of the ambient temperature are transferred inside the camera and towards the detector due to heat conduction and convection. This thermal drift affects the sensor's temperature-dependent pixel responsivity and offset voltage, and detected radiant flux derived from the camera interior. Figure 1 illustrates the composition of the detected radiation and the temperature influences during the measurement.

The thermal drift influences have huge effect on the absolute temperature measurement uncertainty and the spatial deviation of the pixel values if the camera looks at a homogeneous radiation source. In order to achieve low measurement uncertainty values the pixel signal voltages have to be corrected in respect to the present thermal conditions during the measurement. For the proposed calibration method a heating chamber is used to simulate possible ambient temperature changes. During the calibration procedure the correction coefficients are determined which consider the temperature-dependent sensor parameters and estimates of the disturbing camera radiation using additional temperature probes placed inside the camera housing. This method combines experiences of our previous works on calibration of infrared cameras with shutters [3] and shutter-less infrared cameras using temperature-stabilized microbolometer FPAs [5].

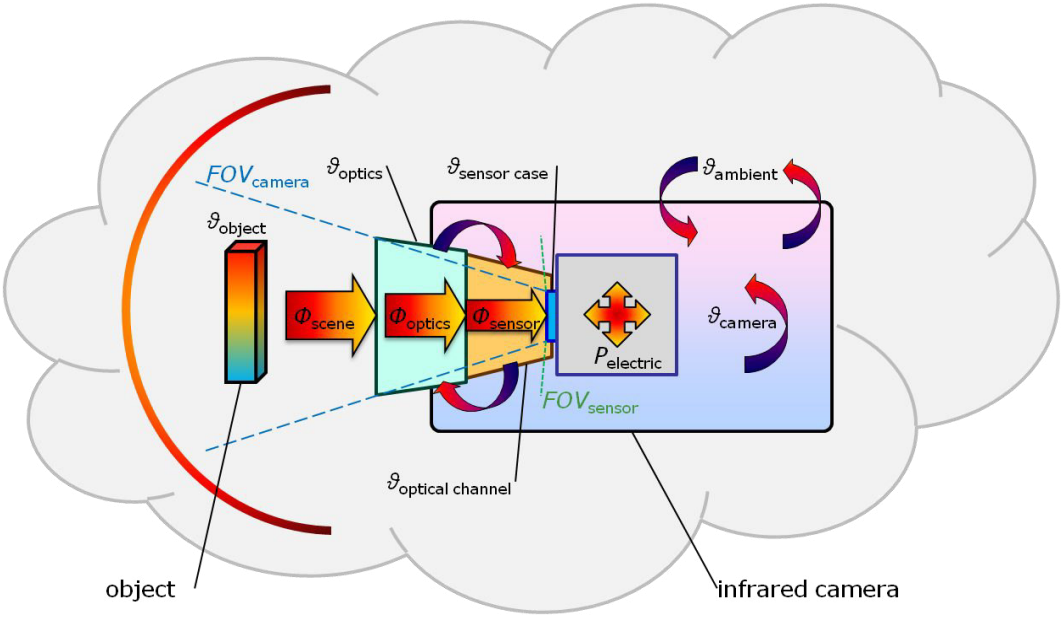


Figure 1. Model of an infrared camera comprising sensor, optics, housing, electronics and measurement environment [1]. $\vartheta_{\text{object}}$ is the object temperature, $\vartheta_{\text{optics}}$, $\vartheta_{\text{sensor case}}$, $\vartheta_{\text{optical channel}}$, $\vartheta_{\text{camera}}$, $\vartheta_{\text{ambient}}$ are the temperature of the optics, the sensor case and so on. $FOV_{\text{sensor}}$ and $FOV_{\text{scene}}$ illustrate the fields of view of the sensor and the camera. $P_{\text{electric}}$ is the thermal losses.

## 3. INFRARED CAMERA

The calibration procedure will be explained for an infrared camera based on a ULIS microbolometer sensor array without temperature stabilization (Tab. 1) [9].

Table 1. Properties of the used infrared camera.

| | |
|---|---|
| **Sensor type** | UL03162-028 (ULIS, France) |
| **TEC** | w/o |
| ***NETD*** | < 100 mK (F/1, 300K, 50Hz) |
| **Resolution** | 384 x 288 |
| **Pixel pitch** | 25 µm |
| **Uniformity (deviation)** | < 1.5% |
| **Power consumption** | < 100 mW |
| ***f*-number** | 1.0 |
| **Focal length** | 18 mm |

The sensor temperature is measured and provided by the detector itself. It is assumed that the sensor temperature is uniformly distributed over all pixels. The sensor specification describes the sensor temperature dependency of the pixel offset voltage with a polynomial of the third order:

$$V_0\left(\vartheta_{fpa}\right) = v_0 + v_1\vartheta_{fpa} + v_2\vartheta_{fpa}^2 + v_3\vartheta_{fpa}^3\,, \tag{4}$$

and the sensor temperature dependency of the pixel responsivity with a polynomial of the second order:

$$R_V\left(\vartheta_{fpa}\right) = r_0 + r_1\vartheta_{fpa} + r_2\vartheta_{fpa}^2\,. \tag{5}$$

Three temperature probes (LM61, Texas Instruments, USA) are placed inside the camera housing in order to capture the thermal state. These four temperatures, three camera and the sensor temperature form the correction input and are continuously captured during the measurements. Figure 2 shows the positions of the temperature measurements.

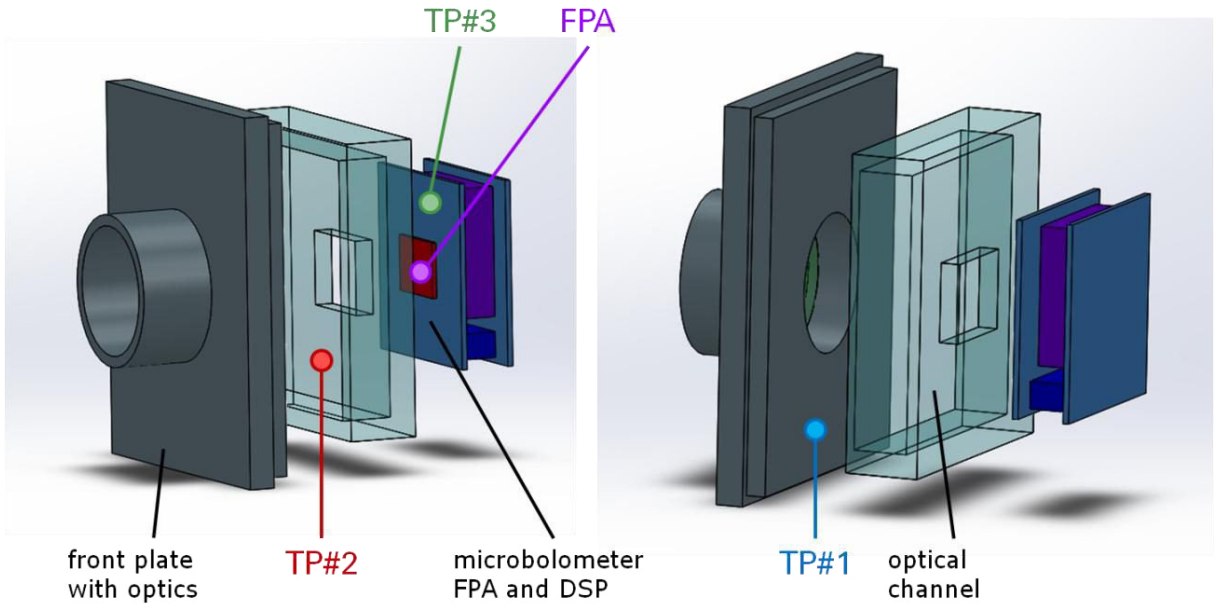


Figure 2. Positions of the temperature measurements inside the camera housing and the detector. TP#1 (blue) is placed on the front plate carrying the optics. TP#2 (red) is located on the front side of the optical channel. TP#3 (green) is placed close to the detector and the signal processing unit on the back side of the optical channel. The fourth temperature measurement is done by the sensor array itself.

To analyze the temperature inputs in respect to their temporal response and the relation between each other the infrared camera was placed inside a heating chamber with controlled chamber temperature. The applied heating and cooling regimes controlled the chamber temperature between 5 °C up to 50 °C in steps of 5 K. Figure 3 depicts the relation between the temperatures in the steady state and compares the time constants.

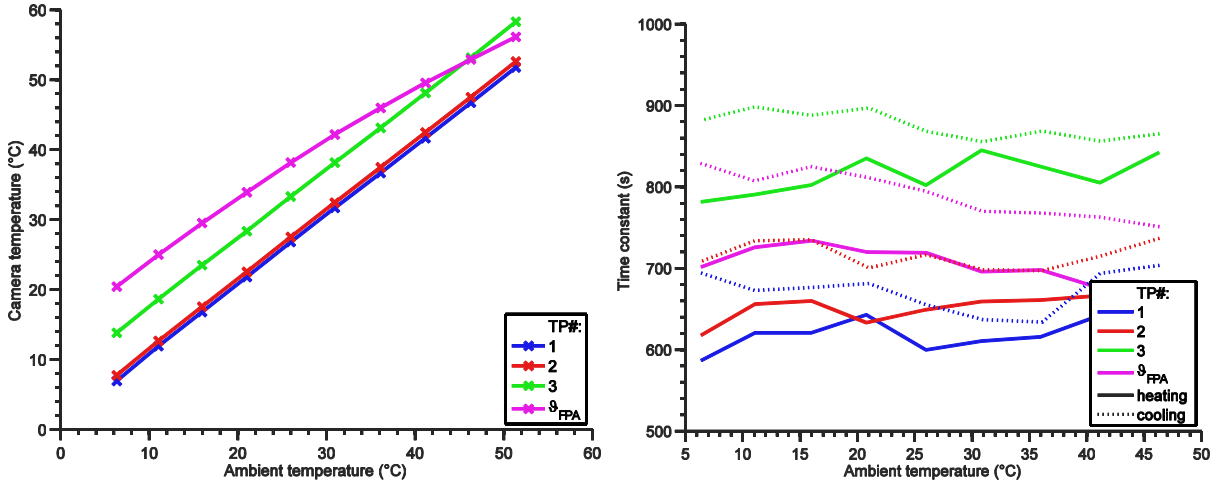


Figure 3. Temporal response of the used temperature correction inputs. Relation between the ambient temperature and the three camera temperatures as well as the sensor temperature in steady-state conditions (left). Only the camera temperatures show linear relation. Time constants of the different temperature probes during the stepwise heating and cooling procedure (right).

The camera temperatures are linearly correlated to the ambient temperature. The increase of the sensor temperature declines with higher temperatures. This might be due to detector-internal compensation processes which lead to less power consumption and thermal losses and, hence, lower sensor temperature values. The time constants of the camera temperatures seem to be independent from the ambient temperature. In case of the sensor temperature a slight decrease of the time constant with higher ambient temperatures can be noted. This might be another sign for internal compensation processes. Apart from this, all time constants during the heating regime are lower compared to the cooling regime.

The signal voltage shows a response almost at the same time as the chamber temperature begins to change. The response times of the temperature probes indicate how fast temperature changes occur. TP#1 responses at first with 39 s delay to the ambient temperature. TP#2 follows after 66 s and TP#3 with 105 s response time. The sensor temperature begins to change after 66 s.

In the steady state only the camera temperatures are linearly correlated with the ambient temperature. The temperature probes and the sensor temperature provide different temporal information about present temperature changes due to staggered response times and time constants. The proposed correction should benefit from these additional temperature information compared to the compensation approach in [6] based only on the sensor temperature.

## 4. CALIBRATION

During the calibration changing external conditions are simulated using a heating chamber in order to determine the correction coefficients. The infrared camera is placed inside this heating chamber looking through a sidewise opening at different blackbodies or testing scenes (Fig. 4).

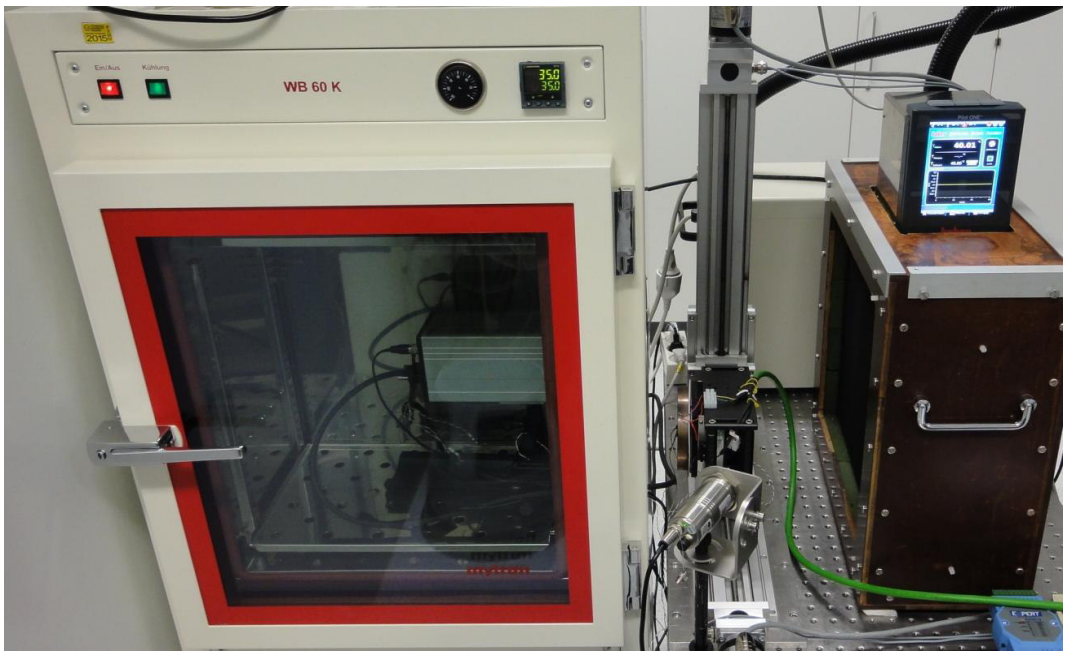


Figure 4. Calibration set-up comprising the heating chamber (left) with the infrared camera inside and a sidewise opening, and one large panel blackbody (right) positioned in front of the opening. A second small circular blackbody (middle) can be moved in front of the camera.

The proposed compensation approach consists of three steps: (i) non-uniformity correction (NUC), (ii) correction of the sensor's temperature-dependent responsivity changes and (iii) offset correction based on the sensor and the camera temperatures. The corrected pixel signal voltages are converted into temperature values according to a radiometric calibration transfer function [3] afterwards. Each calibration step is followed by a bad-pixel replacement procedure.

Blackbodies are radiation sources with low spatial and temporal variations of their controlled surface temperature. Their quality limits the achieved measurement uncertainty of the calibrated infrared camera. The changes of the raw signal voltage due to thermal drift influences are pixel-dependent or cannot be measured separately (see Eqs. (2), (3)). For that

reason, the radiation part derived from the observed scene should be uniform over the entire camera FOV during each calibration step. The correction of the pixel responsivity $R_{V,ij}$ needs two different radiation sources with a known constant temperature difference which can be switch. Two different panel blackbodies were used: (i) a rectangular water bath blackbody with a radiant surface of 350 mm x 350 mm and (ii) a circular copper plate blackbody with a coated radiant surface of 120 mm diameter that can be moved in-between the infrared camera and the other blackbody. Both blackbodies cover the entire field of view of the camera. The delay between two consecutive measurements amounts to 45 s.

**Non-uniformity correction**

The NUC equalizes small variations of the pixel parameters (responsivity and offset voltage) and the different pixel responses due to the pixel-dependent projected solid angle $\omega_{fov,ij}$ (see Eq. (3)) [3]. The input data are at least two raw infrared images of a panel blackbody covering the entire camera FOV at the thermal steady state. The ambient conditions during the capture of the input data should be constant since only the pixel variations related to the object radiation are determined. A standard two-point-NUC is sufficient because of the linear relation between radiation and signal voltage (see Eq. (2)). The correction using the two coefficient matrices $gain_{ij}$ and $off_{ij}$ yields (Fig. 5):

$$V_{nuc,ij} = gain_{ij} V_{raw,ij} + off_{ij} \,. \tag{6}$$

After this correction all pixels follow the same response curve. However, this uniform response is related to specific thermal conditions $(\vartheta_{amb}, \vartheta_{cam}, \vartheta_{fpa})$ outside and inside the camera. These captured temperature values form the set of reference temperatures of the NUC correction coefficients. Changes of these thermal conditions and their effects on the temperature measurement are treated in the next correction steps.

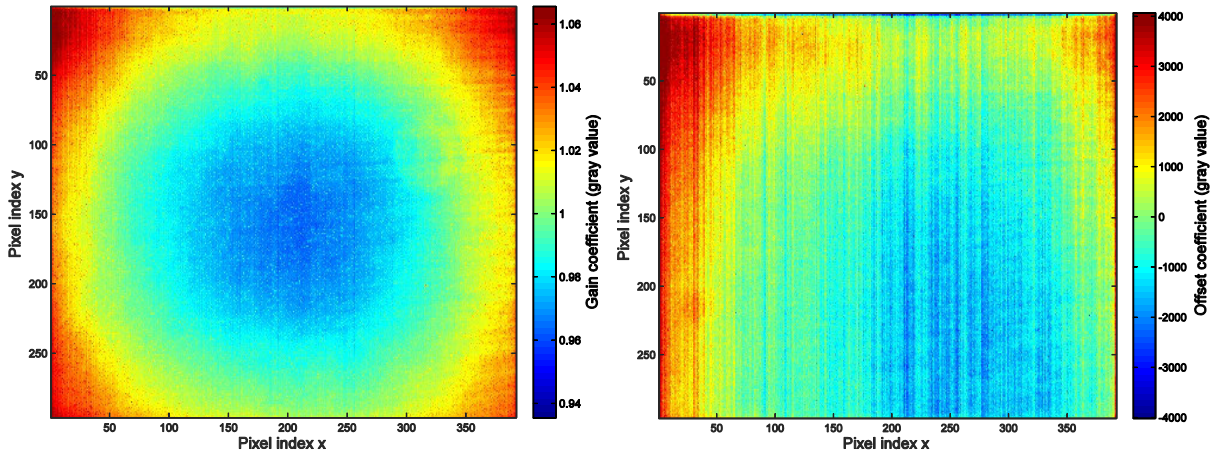


Figure 5. NUC coefficient matrices $gain_{ij}$ (left) and $off_{ij}$ (right). Central symmetric shape of $gain_{ij}$ is due to the relation to the pixel-dependent projected solid angle $\omega_{fov,ij}$ related to the object radiation. Variations in the offset values show no correlation.

**Responsivity correction**

The assumed all-time uniform sensor temperature results in equal responsivity changes for all pixels. But it is not possible to distinguish parts of the signal voltages related to different portions of radiation according to their origin, or to illuminate all pixels with the same radiant flux density. For that reason and due to a pixel-dependent projected solid angle $\omega_{fov,ij}$, the responsivity changes are pixel-dependent. The difference signal voltage $\Delta V_{obj,ij}$ depends on the pixel responsivity $R_{V,ij}$, the pixel area $A_{pix}$, the projected solid angle $\omega_{fov,ij}$ and the radiant exitance difference $\Delta L_{obj}$:

$$\Delta V_{obj,ij}\left(\vartheta_{fpa}\right) = R_{V,ij}\left(\vartheta_{fpa}\right) \cdot A_{pix} \omega_{fov,ij} \Delta L_{obj} \,. \tag{7}$$

The chamber temperature is controlled between 15 °C and 50 °C and follows a defined time regime (Fig. 6). During the calibration both blackbodies are switched periodically. The time difference between two consecutive measurements of the same radiation source amounts to 90 s due to the motion time of the small panel blackbody. To consider these

temporal deviations time-based averaging could be used in order to get quasi-simultaneous measurements. However, during the transition time towards the new ambient temperature high measurement uncertainty values were observed. For that reason, only the steady-state measurements were used for the regression. Figure 6 shows the measured difference signal voltage $\Delta V_{obj,ij}$ versus the sensor temperature $\vartheta_{fpa}$ for three sample pixels with different distances from the optical axis. The curves have different slopes and cross each other at the reference sensor temperature due to the previously applied NUC. A polynomial of the second order is sufficient for regression:

$$g_{V,ij}\left(\vartheta_{fpa}\right) = 1 + g_{1,ij}\vartheta_{fpa} + g_{2,ij}\vartheta_{fpa}^2 . \tag{8}$$

The normalized regression function $g_{V,ij}$ is used to correct the NUC signal voltage $V_{nuc,ij}$:

$$V_{G,ij} = \frac{V_{nuc,ij}}{g_{V,ij}\left(\vartheta_{fpa}\right)} . \tag{9}$$

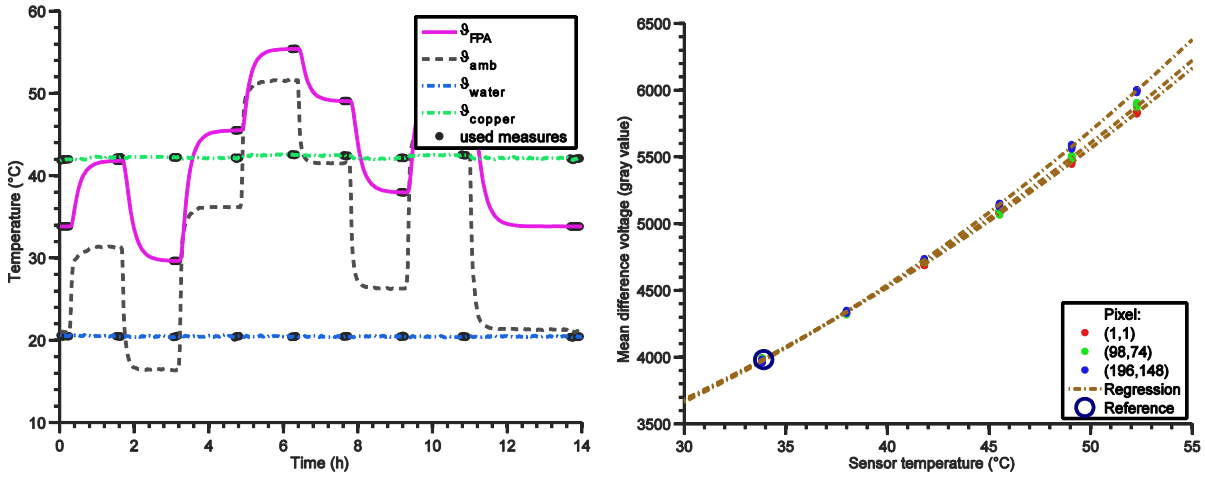


(a) (b)

Figure 6. (a) Observed temperatures during the responsivity calibration step. The ambient temperature $\vartheta_{\mathrm{amb}}$ is controlled between 15 °C and 50 °C and the sensor temperature $\vartheta_{\mathrm{fpa}}$ follows that changes. The two blackbody temperatures $\vartheta_{\mathrm{water}}$ and $\vartheta_{\mathrm{copper}}$ are constant. (b) Difference signal voltage versus sensor temperature of three sample pixels at the corner of the FPA (red), in the middle (blue) and in-between (green). The circle marks the reference sensor temperature from the NUC where the different curves cross each other. Dashed lines depict the regression curves used for the pixel responsivity correction.

**Offset voltage correction**

In [4] the compensation of changing disturbing camera radiation has been studied based on temperature measurements inside the camera housing and using temperature-stabilized sensor arrays. Infrared cameras comprising FPAs without temperature stabilization makes the offset correction more complex since the pixel offset voltage $V_{0,ij}$ and the radiant exitance $M_{pix}$ depend on the sensor temperature (see Eqs. (2), (3)). Due to the close correlation between the camera temperature and the sensor temperature it is not possible to determine the different correction parameters separately. However, the different temporal responses of the temperature correction inputs shown in section 3 allow to distinguish partially between these influences. For that reason, a second temperature time regime is applied on the infrared camera looking at the water bath blackbody at constant temperature (Fig. 7).

The four correction inputs are used for the regression of the pixel signal voltages after applied responsivity correction. Second-order polynomials are sufficient for the relation between the signal voltage and the temperatures TP#1…3. A polynomial of the third order is needed for the regression based on the sensor temperature and agrees with the manufacturer's specification. The individual steady-state regressions are combined to a more complex regression model which allows to estimate the behavior during transient thermal conditions. Additional information about the temperature distribution inside the camera is provided by the time derivatives of the camera temperatures and cross-correlation coefficients formed by multiplying two or more camera temperature inputs [5]. The final regression model is composed

of the following three groups of inputs: (i) absolute temperatures, (ii) time derivatives and (iii) cross-correlation of temperature inputs. The resulting correction based on the regression function $o_{V,ij}$ yields:

$$V_{O,ij} = V_{G,ij} - o_{V,ij}\left(\vartheta_{fpa}, \dot{\vartheta}_{fpa}, \vartheta_{TPm}, \dot{\vartheta}_{TPm}, \vartheta_{fpa}\cdot\vartheta_{TPm}, \vartheta_{TPm}\cdot\vartheta_{TPn}\right). \quad (10)$$

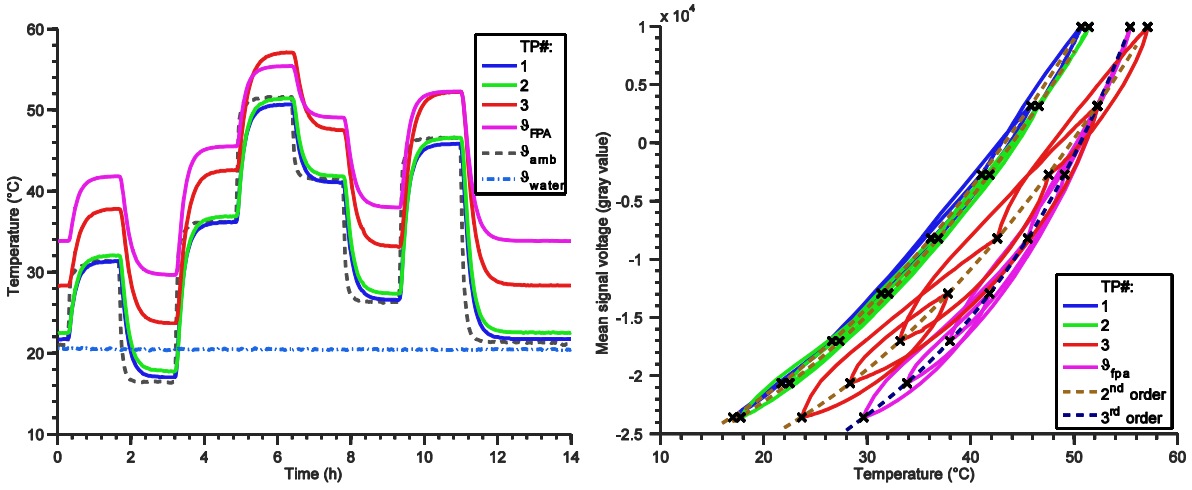


(a) (b)

Figure 7. (a) Temporal responses of measured temperatures representing the thermal state during the offset calibration regime. The set of correction input temperatures from TP#1…3 and the sensor temperature $\vartheta_{fpa}$ follow the changes of the ambient temperature $\vartheta_{amb}$. The blackbody temperature $\vartheta_{water}$ is kept constant. (b) Mean signal voltage after responsivity correction versus the four correction inputs (TP#1…3, sensor temperature) during offset calibration regime. Black crosses mark the steady-state conditions used for the regression (dashed lines).

Table 2 compares the correction results of different compositions of temperature inputs. The temporal standard deviation of the mean corrected signal voltage $\sigma_t$ and the mean spatial standard deviation from the mean signal voltage $\sigma_s$ provide information about correction uncertainty. The time derivative inputs are more important than the cross-correlation. It can be seen that the more input temperatures are used the better are the correction results.

**Voltage to temperature conversion**

The relation between the corrected signal voltage $V_{O,ij}$ and the surface temperature $\vartheta_{obj}$ of the observed object can be approximated using a second-order polynomial. However, in [3] it is presented how the approximation uncertainty can be reduced especially outside the supporting points using a Planck-like approximation function based on four coefficients $r, b, f$ and $o$:

$$V_{O,ij} = \frac{r}{e^{\frac{b}{\left(\vartheta_{obj}+273.15\right)}} - f} + o\,. \quad (11)$$

After determining the regression coefficient the inverted function defines the voltage-to-temperature conversion function:

$$\vartheta_{O,ij} = \frac{b}{\ln\left(\frac{r}{V_{O,ij}-o}\right)+f} + 273.15\,. \quad (12)$$

The correction results from above are usually given in temperature values (see Tab. 2).

Table 2. Comparison of correction results after offset compensation using different numbers of temperature inputs.

| **Temperature input** | **Residual temporal standard deviation $\sigma_t$ of the mean corrected pixel signal voltages** | | **Residual mean spatial standard deviation $\sigma_s$ of the corrected pixel voltages (gray value)** | | **Number of coefficients for offset correction function** |
|---|---|---|---|---|---|
| | (gray value) | (mK) | (gray value) | (mK) | |
| $\vartheta_{fpa}$ | 498.7 | 2942.2 | 17.0 | 100.7 | 4 |
| $\vartheta_{fpa}, \vartheta_{TPm}$ | 24.0 | 141.9 | 7.3 | 43.2 | 10 |
| $\vartheta_{fpa}, \dot{\vartheta}_{fpa}, \vartheta_{TPm}, \dot{\vartheta}_{TPm}$ | 16.3 | 96.6 | 7.1 | 42.3 | 15 |
| $\vartheta_{fpa}, \vartheta_{TPm}, \vartheta_{fpa} \cdot \vartheta_{TPm}, \vartheta_{TPm} \cdot \vartheta_{TPn}$ | 20.1 | 118.9 | 7.1 | 41.9 | 17 |
| $\vartheta_{fpa}, \dot{\vartheta}_{fpa}, \vartheta_{TPm}, \dot{\vartheta}_{TPm}, \vartheta_{fpa} \cdot \vartheta_{TPm}, \vartheta_{TPm} \cdot \vartheta_{TPn}$ | 15.2 | 89.7 | 6.9 | 41.0 | 22 |

## 5. CONCLUSION

In this paper we presented an ambient temperature compensation method for microbolometer-based infrared cameras working without shutter and sensor temperature stabilization. The responsivity and offset correction were based on several temperature inputs representing the thermal state inside the camera. The measurement uncertainty after correction depends primarily on the numbers of considered coefficients for the offset correction function. A temporal mean temperature deviation $\sigma_t$ of 89.7 mK and a mean spatial deviation $\sigma_s$ of 41.0 mK were achieved for the calibration measurement. Another parameter for the correction quality is the correctability $C$ presented in [3]. It is defined by the ration of the spatial standard deviation $\sigma_s$ of the sensor array versus the temporal standard deviation $\sigma_n$ of the corrected pixel signal voltage, which refers to the temporal noise of the pixels:

$$C = \frac{\sigma_s}{\sigma_n} \tag{13}$$

For the proposed correction method this ratio yields $16.9/11.5$. This shows that the spatial uncertainties derived from the variations of blackbody temperatures in space and time dominate the uncertainty of the pixel signal voltage in time. In conclusion, the main drawback of the shutter-less and TEC-less correction is that all correction information has to be determined a priori under simulated ambient conditions. For that reason, the quality of the calibration set-up defines the achievable measurement uncertainty.

## REFERENCES


[1] Budzier, H., Gerlach, G., [Thermal Infrared Sensors], John Wiley & Sons, Chichester (2011).

[2] Tempelhahn, A., Budzier, H., Krause, V., Gerlach, G., "Development of a shutterless calibration process for microbolometer-based infrared measurement systems", Proc. QIRT 2014, 1-10 (2014).

[3] Budzier, H., [Radiometrische Kalibrierung ungekühlter Infrarot-Kameras]. TUDpress, Dresden (2014).

[4] Nugent, Paul W., Shaw, Joseph A., Pust, Nathan J., "Radiometric calibration of infrared imagers using an internal shutter as an equivalent external blackbody", Opt. Eng. 53(12), 123106 (2014).

[5] Tempelhahn, A., Budzier, H., Krause, V., Gerlach, G., "Modeling transient thermal behavior of shutter-less microbolometer-based infrared cameras", Proc. SPIE, Vol. 9249, 924904 -1-9 (2014).

[6] Nugent, P. W., Shaw, J. A., "Calibration of uncooled LWIR microbolometer imagers to enable long-term field deployment", Proc. SPIE, Vol. 9071, 90710V-1-10 (2014).

[7] Olbrycht, R., Wiecek, B., De Mey, G., "Thermal drift compensation method for microbolometer thermal cameras". Applied Optics 51 11, 1788-1794 (2012).

[8] Tempelhahn, A., Budzier, H., Krause, V., Gerlach, G., "Modeling signal-determining radiation components of microbolometer-based infrared measurement systems", Proc. IRS² 2013, 1-5 (2013).
[9] ULIS, "Nano 384P TM", <http://www.ulis-ir.com/uploads/Products/Nano384P-UL03162.pdf>, (August 2012). http://www.ulis-ir.com/index.php?infrared-detector=documentation
[10] Bieszczad, G., Orzanowski, T., Kastek, M., "Method of detectors offset correction in thermovision camera with uncooled microbolometric focal plane array", Proc. SPIE, Vol. 7481, 74810O-1 8 (2009).